Friction

https://doi.org/10.26599/FRICT.2026.9441254

Research Article

A multidimensional investigation of the transition from lubricated to abrasive wear

Yulong Li[1,2]✉, Johannes Schneider[1,2], Christian Greiner[1,2]✉

[1] Institute for Applied Materials (IAM), Karlsruhe Institute of Technology (KIT), Kaiserstrasse 12, Karlsruhe, 76131, Germany.

[2] KIT IAM-ZM MicroTribology Center (μTC), Strasse am Forum 5, Karlsruhe, 76131, Germany.

✉ Corresponding author. E-mail: yulong.li@kit.edu, christian.greiner@kit.edu

Received: November 28, 2025; Revised: January 19, 2026; Accepted: April 9, 2026

Abstract: Abrasive wear is one of the most critical degradation mechanisms in tribological systems, leading to material loss, reduced efficiency, and premature failure of components. Despite its importance, predicting the initiation and progression of abrasive wear remains challenging because the

complex nature of lubrication conditions. In this study, continuous pin-on-disk experiments using bearing steels were conducted to investigate predictive indicators of abrasive wear. During the first 2000 seconds, the contact was lubricated with a base oil to establish stable frictional conditions. At 2000 s, an abrasive slurry was introduced into the contact without interrupting rotation, simulating the sudden intrusion of abrasive particles. Subsequently, the evolution of friction before and after the onset of abrasive wear was analyzed from three complementary perspectives, demonstrating the potential for predictive assessment. First, the spatial distribution of friction on the disk under both lubricated and abrasive wear conditions exhibited similar patterns despite the large difference in magnitude, suggesting that friction measured in the lubricated regime already reflects the inherent spatial structure of the contact and can therefore indicate where high friction and wear are likely to occur. Second, wavelet analyses of friction signal successfully revealed transient features in the frequency domain that are associated with the initiation of abrasive wear, with spectral responses appearing before the increase in friction. Third, precontact measurable parameters, namely, disk surface topography and disk tilting induced oscillations, were found to be effective indicators for predicting high friction regions. These three approaches provide a framework for forecasting, detecting, and understanding abrasive wear, thereby contributing to the development of intelligent predictive maintenance strategies in tribological systems.

Keywords: Abrasive wear, friction prediction, wear prediction, time frequency analysis

1 Introduction

Reducing energy consumption associated with friction and wear is a cornerstone of modern sustainable engineering. Recent global analyses have shown that nearly 23 % of total energy consumption

originates from friction and wear processes, while about 1.4 % of the world's GDP could be saved annually through advanced tribological technologies [1]. Improving tribological performance therefore represents a direct pathway toward energy efficiency and carbon neutrality. Among various tribological phenomena, abrasive wear plays a particularly destructive role, often dictating the service life and reliability of critical components such as bearings, seals, and gears [2–4]. The unexpected onset of abrasive wear, caused by the intrusion of hard particles into lubricated contacts, remains one of the leading causes of premature mechanical failure [5]. Therefore, the ability to predict frictional behavior and abrasive wear, under lubrication or before high friction occurs, would be highly desirable.

Due to the importance of abrasive wear, extensive research efforts have been devoted to its investigation over the years, leading to significant progress across multiple length scales through both experimental and modeling approaches. Analytical relations such as Archard's law [6] established a foundation for describing the wear volume as a function of load and sliding distance. Building on these classical principles, advanced continuum models have been developed to simulate particle surface interactions and material removal during abrasive wear [7]. Experimental studies have revealed the morphology and evolution of wear particles and surface topography under varying conditions [8, 9], while recent combined simulation and experiment studies have explored dynamic abrasive behavior in lubricated contacts [10].

In parallel, the rapid growth of data driven tribology has opened new perspectives for abrasive wear and friction prediction. This emerging paradigm shift, as highlighted in several recent comprehensive reviews, moves the field toward a systematic integration of materials design, experimental data, and real-time condition monitoring [11–13]. The foundation of this trend lies in the implementation of FAIR (Findable, Accessible, Interoperable, and Reusable) data solutions, which provide the robust infrastructure necessary for applying artificial intelligence (AI) to complex contact problems [14]. A

current insightful study introduced an active learning framework for nonparametric multiscale modeling of boundary lubrication, in which molecular dynamics and continuum simulations are coupled through Gaussian process regression [15]. This method enables refinement of interfacial constitutive behavior and captures transitions in boundary lubrication without predefined empirical models. On the computational front, AI based prediction has demonstrated its strong potential for solving engineering scale tribological problems. For example, by employing support vector machines, gaussian process regression, and neural networks to predict elastohydrodynamic lubrication (EHL) film thickness parameters directly from full-system finite-element data, achieving about 25 times faster than finite element EHL simulations and with higher accuracy and flexibility [16]. Another work used experimental data combined with neural network optimization to model friction and wear in ball-on-flat contacts under mixed lubrication. With only two independent datasets, the model accurately reproduced the evolution of contact and pressure distributions [17].

Meanwhile, time frequency analysis offers an additional perspective for studying tribological contacts. Techniques such as Continuous Wavelet Transform (CWT), Short Time Fourier Transform, and Hilbert Huang Transform enable combined temporal and spectral analysis of friction, vibration, and acoustic signals [18–20]. For example, CWT has proven effective in diagnosing nonstationary machinery faults [21], while wavelet analysis of acoustic emissions enables early detection of wear [20]. These methods provide enhanced sensitivity to lubrication failure due to abrasive wear. With ongoing advances in sensing technologies and artificial intelligence, time frequency analysis for real time tribological diagnostics is expected to become increasingly important [22].

Taken together, while previous studies employing AI and time frequency analyses have significantly advanced the prediction of tribological behavior, lubricated and abrasive regimes are often treated as independent states and rarely incorporate spatial domain information to bridge them. Building upon

these developments, the present study investigates the transition from lubricated conditions to abrasive wear through a multidimensional framework, with the aim of elucidating the interconnections among spatial, temporal, and frequency responses of the tribological system. A continuous pin-on-disk test using 100Cr6 bearing steel was performed, where a base oil provided stable lubrication for the first 2000 s before an abrasive slurry was introduced to simulate a sudden particle intrusion event. The core contribution of this work lies in revealing the surprising spatial consistency between these two regimes: we demonstrate that the inherent spatial structure of a lubricated contact serves as a 'fingerprint' that predefines the locations of subsequent abrasive. By elucidating these cross regime interconnections, this study provides new insights into the mechanisms governing the onset of abrasive wear and its potential predictability.

2 Experimental

2.1 Materials

Tribological tests were conducted using a pin-on-disk setup (in Fig. 1a), where both the pin and disk specimens were bearing steel (100Cr6, AISI 5210). The disks (supplied by Eisen Schmitt, Germany), were 70 mm in diameter and underwent hardening and tempering to attain a target hardness of around 800 HV. Surface finishing was performed on a cup grinding machine (MPS 2 R300, G&N, Germany) using EK200 corundum grinding wheels, yielding a surface roughness between 0.25 and 0.4 μm (R_q, Gauss L-Filter 0.8 mm, ISO 21920) in sliding direction, as determined by a tactile profilometer (T8000 R120-400, HOMMEL ETAMIC, Germany). Flatness along the 132 mm sliding track was maintained below ±3 μm (in Fig. 1b), verified with an optical profiler (TopMap Micro.View$^+$, Polytec, Germany).

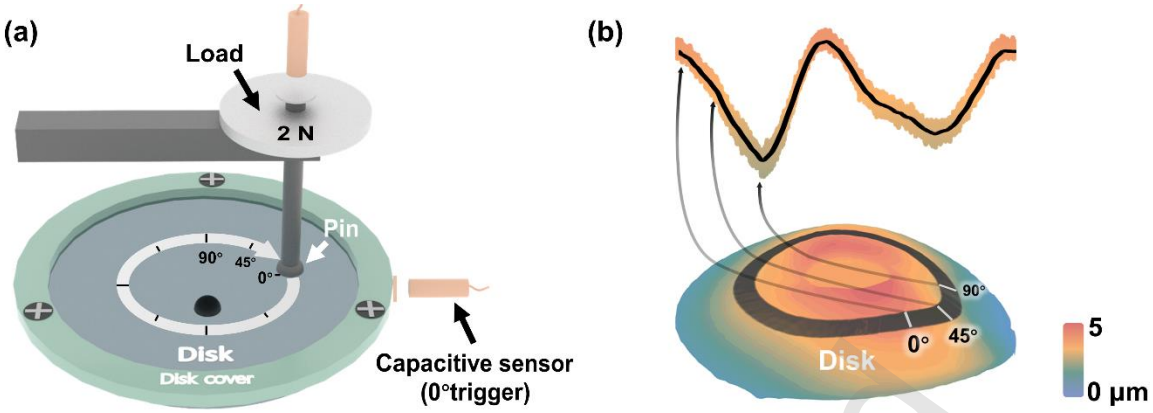

Fig. 1 Schematic diagram of experimental setup and disk surface topography. (a) Experimental setup of the pin-on-disk tribological test. The pin was fixed while the disk rotated counterclockwise. A zero-position trigger was incorporated to segment the data corresponding to each revolution of the disk. (b) Extraction of the surface profile of the sliding track from the optical profiler, the height difference (flatness) along the 132 mm sliding track is approximately 3 μm.

The spherical pins, 8 mm in diameter, were flattened on one side to form a circular contact area with a diameter of 7.33 mm, and were employed in their as received condition (supplied by KGM, Germany). These pins had an average hardness of approximately 700 HV, with the flattened surfaces showing roughness (R_q, Gauss L-Filter 0.8 mm, ISO 21920) values in the range between 0.2 and 0.3 μm and a flatness below 0.6 μm. Both pins and disks were demagnetized and ultrasonically cleaned in isopropanol for 15 minutes before test to eliminate surface contaminants.

An additive free mineral base oil (FVA1, Klüber, Germany) with a dynamic viscosity of 0.066 pa·s at 24 °C was selected to create lubricated conditions. To simulate an abrasive environment, aluminum oxide slurry (BIOLAM®, Joke, Germany) containing 12.5 wt.% Al_2O_3 particles with a nominal size of 5 μm (FEPA standard) was employed, the dynamic viscosity and particle size distribution can be found in Supplementary Note 1.

2.2 Tribological testing

Tribological experiments were carried out using a custom modified pin-on-disk tribometer with dead weight loading (in Fig. 1a), initially developed by the Swiss Center for Electronics and

Microtechnology and currently owned by Anton Paar (Switzerland). The pin-on-disk tribometer underwent adaptation to include a side mounted capacitive sensor and a coaxially aligned metal block attached to the rotating disk, offering frictional data with full spatial resolution along the sliding track, with friction force resolution of 0.06 mN. Each complete rotation was marked by the passage of the metallic block over the sensor, which generated a trigger signal. As illustrated in Fig. 2a, the disk was securely positioned and aligned before each test using three screws on a specially designed holder with a spherical base. The oscillation amplitude (alignment accuracy) along the wear track was constrained to around 6 µm (according to a flatness of ±3 µm) in Fig. 2b, evaluated from the capacitive sensor data located above of the contact zone in Fig. 2a.

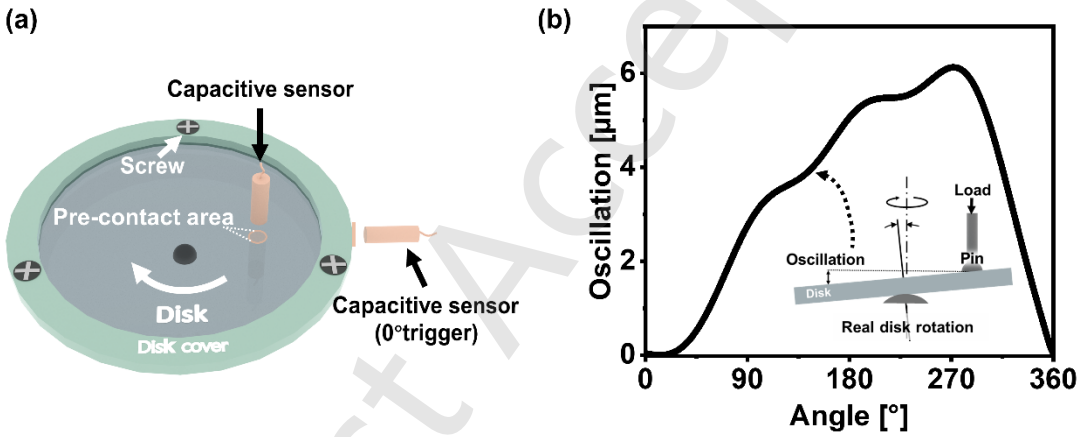

Fig. 2 Schematic diagram of disk mounting setup and tilting induced oscillation. (a) before the tribological contact, the disk was mounted and leveled using three screws on the disk cover with a spherical base, while a capacitive sensor recorded the height variations (oscillation) of the sliding track during rotation. (b) The oscillation amplitude along the sliding track was strictly limited to approximately 6 µm.

In the tribological experiments, a data acquisition rate of 1000 Hz was used, with a normal load of 2 N and a sliding speed of 50 mm/s. To establish lubricated conditions, 5 ml of an additive free mineral base oil was introduced into the setup prior to each test. After 2000 s of sliding (equivalent to a distance of 100 m), an additional 5 ml of Al_2O_3 abrasive slurry was added to induce abrasive wear, and therefore study the transition from lubrication to abrasive wear. The abrasive slurry was supplied using a syringe connected to a delivery tube, the outlet of which was fixed above the tribological contact, at the 180°

position in Fig. 2. The outlet of the tube did not come into contact with any components involved in the experiment. At 2000 s, the syringe was rapidly actuated, allowing the abrasive slurry to enter the contact zone through the tube outlet.

2.3 Surface topography

The surface topography characterization consisted of two parts. First, the spatial distribution of roughness R_q (Gauss L-Filter 0.8 mm, ISO 21920) along the sliding track was measured every 15° in the radial direction using a stylus profilometer (T8000 R120-400, HOMMEL-ETAMIC, Germany). Second, in addition to capturing frictional data with full spatial resolution along the sliding track, the corresponding surface topography was also considered. Achieving complete high resolution surface measurements over such an extended sliding track (132 mm) is typically challenging. To address this, a white light interferometer (TopMap Micro.View+, Polytec, Germany) equipped with a 0.6× objective lens was employed. This configuration enabled the reconstruction of the entire 70 mm diameter disk surface with minimal stitching, from which the full topography of the sliding track could subsequently be extracted, as shown in Fig. 1b.

2.3 Worn surface

Surface topography of both unworn and worn areas was characterized using the 0.6x objective, and further high-resolution measurements were conducted with 10x and 50x lenses to enable more detailed surface information. Microstructural analysis and worn surface characterization were also carried out using a dual beam focused ion beam/scanning electron microscope (FIB/SEM; Helios NanoLab DualBeam 650, FEI, Hillsborough, USA). The worn regions of the disk were observed via scanning electron microscopy.

2.4 Time frequency analysis

The friction force signal *x(t)* was sampled at 1000 Hz, and a continuous wavelet transform (CWT) with the analytic Morlet mother wavelet was applied. The frequency range of 0.1-100 Hz was chosen to capture physically meaningful friction induced dynamics while excluding ultra low frequency drift and high frequency noise. A high voices per octave value (48) was used to ensure sufficient low frequency resolution. The CWT of friction force signal x(t) is defined as [23, 24]:

$$W_x(a,b) = \frac{1}{\sqrt{|a|}} \int_{-\infty}^{\infty} x(t) \psi \left(\frac{t-b}{a} \right) dt$$

where the scale factor *a* adjusts the degree of the wavelet, thereby enabling the analysis of different frequency components of the signal. The translation factor *b* shifts the wavelet along the time axis, ensuring that the entire signal duration is covered during the analysis.

And the corresponding wavelet power is:

$$P = |W_x(a,b)|^2$$

To emphasize relative changes in spectral content over time, the wavelet power was normalized every time slice. At each time instant, all frequency components were divided by the maximum power value of that column:

$$\bar{P} = \frac{P(t)}{\max P(t)}$$

3 Results

3.1 Friction

The evolution of the friction force over time is shown in Fig. 3a. The black line represents the friction force, calculated as the average value over each second (corresponding to about one-third of a

revolution). The transparent shaded region denotes the statistical standard deviation, referred to as frictional fluctuations in this manuscript. During the lubricated condition (before 2000 s), where only the base oil was present at the interface, the friction force remained low at approximately 0.07 N, with maximum fluctuations around 0.03 N. Following the introduction of the abrasive slurry at 2000 s, the friction force did not increase immediately. Instead, a pronounced rise in the friction force was observed after approximately 80 s, eventually reaching a value of around 0.25 N, with maximum frictional fluctuations approaching 0.2 N.

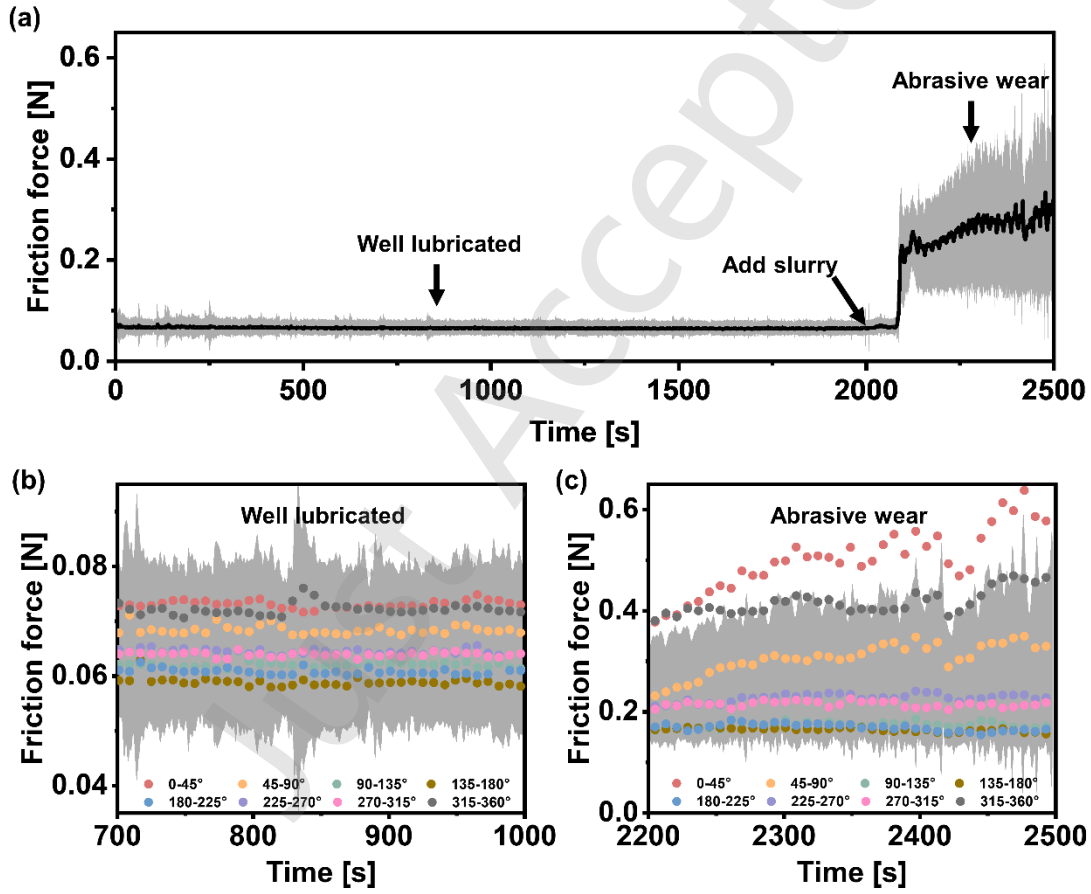

Fig. 3 Friction force in the time domain. (a) The overall time evolution of friction during the entire experiment. The black line represents the mean friction force, and the transparent gray band indicates the standard deviation. Before 2000 s, the system operated in lubricated conditions with a base oil. At 2000 s, an abrasive slurry was introduced. (b) and (c) show the variation of friction in both time and spatial dimensions under (b) lubricated condition (700-1000 s) and (c) abrasive wear condition (2200-2500 s). The dashed lines represent the temporal evolution of friction at different sections along the disk.

By modifying the tribometer (as illustrated in Fig. 1a), the spatial resolution of the friction force along the sliding track was enabled. Accordingly, in Fig. 3b and c, the 360° sliding track was divided into eight sections (each 45°, as illustrated in Fig. 1a), and the friction force was calculated separately for each section. These spatially resolved values were then plotted over the standard deviation of the time-resolved frictional data. The results revealed that, between 700-1000 s (lubricated condition) and 2200-2500 s (abrasive wear condition), the friction force exhibited a non-uniform distribution along the track. Interestingly, certain spatial patterns remained consistent across both conditions, for example, the regions between 0°-45° and 315°-360° consistently showed higher friction, while the 180°-225° sector maintained lower friction throughout.

In Fig. 4, the average friction force was calculated at a higher spatial resolution by evaluating data every 3° along the sliding track, e.g., the value at 1.5° represents the average from 0° to 3°. The analysis was performed using data from the same intervals as in Fig. 3a, 700-1000 s for the lubricated condition and 2200-2500 s for the abrasive wear one. The higher spatial resolution further reveals that the friction distribution along the sliding track under abrasive wear conditions closely resembles that observed under lubricated conditions.

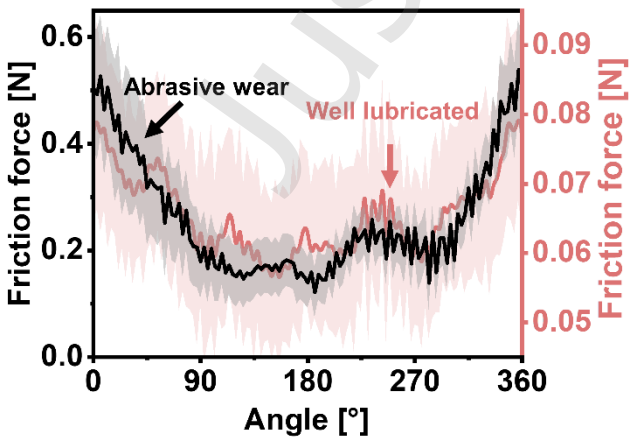

Fig. 4 Friction force in the spatial domain. Comparison of the angularly resolved friction under lubricated and abrasive wear conditions. The data were obtained from the time intervals of 700-1000 s and 2200-2500 s, respectively, corresponding to the same periods shown in Figures 3b and 3c. For spatial resolution, the friction data were averaged every 3°, e.g., the value at 1.5° represents the average

from 0° to 3°. The transparent gray band indicates the statistical standard deviation of the corresponding angular region over the entire analyzed time period.

3.2 Friction and surface topography

Fig. 5a shows the variation of roughness R_q and friction force (from 700-1000 s) as a function of angular position along the sliding track. The roughness R_q fluctuates between approximately 0.28 μm and 0.36 μm, while the friction force remains within the range of 0.06-0.09 N. No clear correlation is observed between the two curves. Fig. 5b presents the variation of the surface profile and friction force with angular position. Two peaks appear in the surface profile, and one of them coincides with a region exhibiting relatively high friction (around 0°).

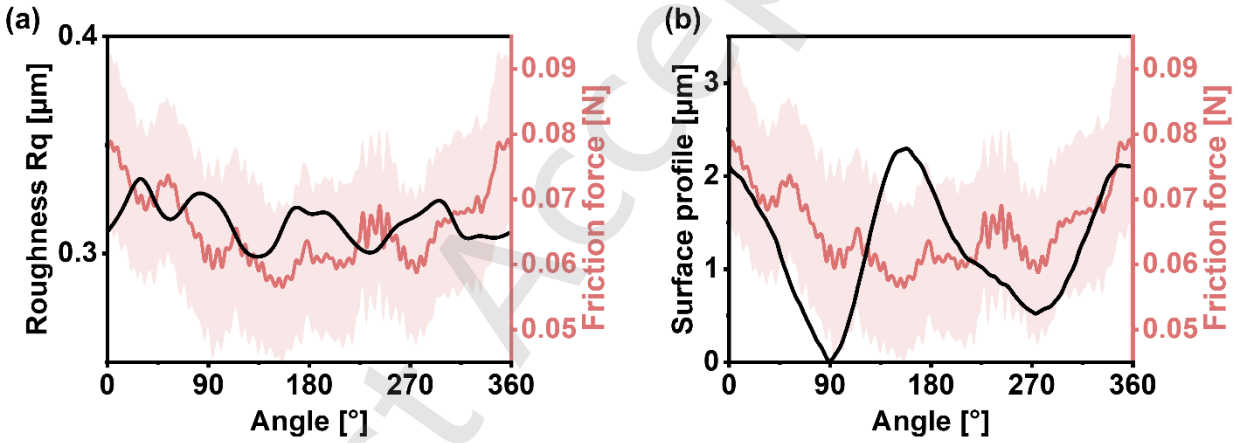

Fig. 5 Friction and surface topography. (a) Comparison of friction and roughness R_q in the spatial domain. The roughness distribution along the sliding track was measured every 15° in the radial direction using a stylus profilometer. (b) Comparison of friction and surface profile along the sliding track.

3.3 Wear

Fig. 6 presents the surface topography before and after the tribological experiments for two regions along the sliding track, located around 0° and 180°, respectively. These regions correspond to the locations of high and low friction forces identified in the spatial domain (Fig. 4). Before the test, the surface along the sliding track exhibited a uniform texture characterized by grinding induced grooves,

in Fig. 6a and d. These grooves maintained a consistent orientation relative to the sliding direction, forming a fixed angle of approximately 60°, which remained constant throughout the track.

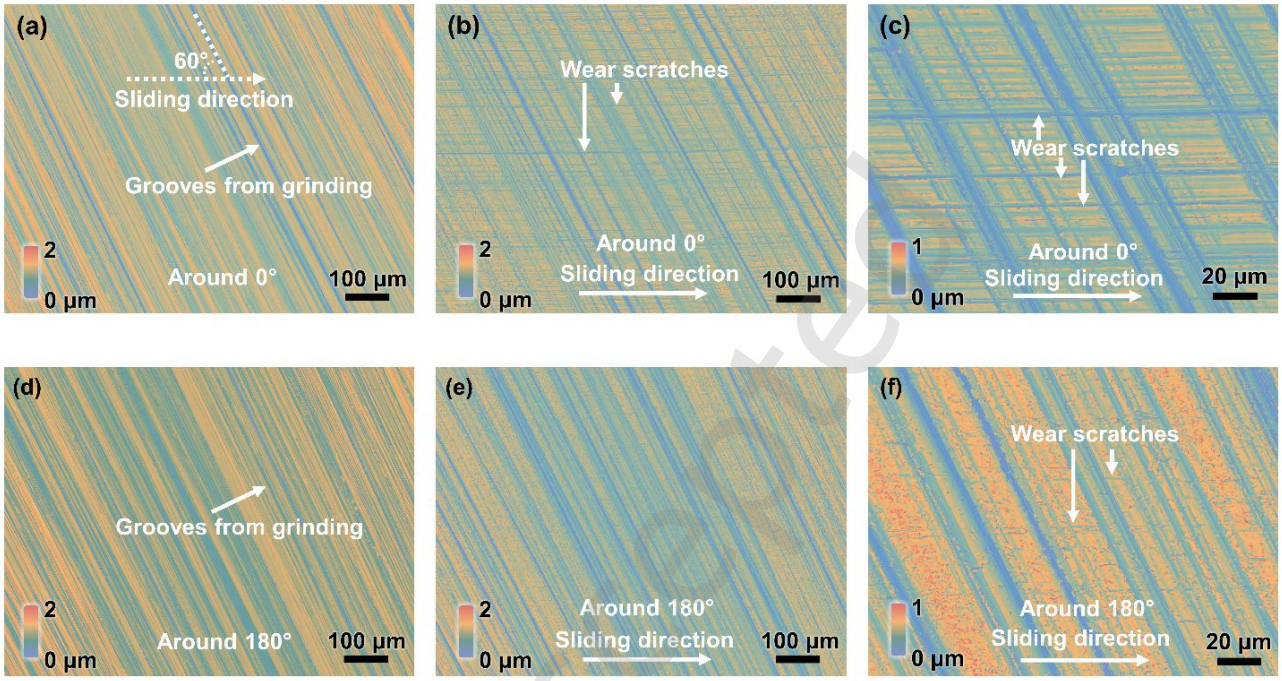

Fig. 6 Surface topography before and after the tribological tests. (a-c) correspond to the high friction region around 0°, as identified in the spatial friction map shown in Fig. 4. (d-f) correspond to the low friction region around 180°. (a) and (d) show the surface topography before the test, measured using a 10× objective. (b) and (e) show the surface topography after the test, also obtained with a 10× objective. (c) and (f) present magnified views of (b) and (e), respectively, acquired using a 50× objective.

The surface topography revealed distinct differences between high and low friction regions. With the 10x objective of the white light interferometer, the high friction region (around 0°, in Fig. 6b) exhibited numerous wear scratches aligned parallel to the sliding direction. In contrast, in the low friction region (around 180°, in Fig. 6e), no prominent scratches were observed at this resolution. With increasing magnification and the 50x objective, this contrast remained evident: at higher resolution, the high friction area (in Fig. 6c) showed pronounced and continuous wear scratches along the sliding direction, whereas the low friction region (in Fig. 6f) displayed only shallow, discontinuous wear scratches along the sliding direction.

Fig. 7 presents SEM images of the high and low friction regions (around 0° and 180°, respectively) after 2500 s (125 m) of sliding, corresponding to the same locations shown in Fig. 6. These images were selected to examine the wear characteristics of surfaces exhibiting markedly different frictional behavior. In Fig. 7a, in the direction parallel to sliding, dense wear scratches are clearly visible. Additionally, the grinding induced grooves present prior to the tribological test have progressively faded, with some nearly worn away. The worn surface shown in Fig. 7b differs significantly from that in Fig. 7a. In Fig. 7b, no continuous wear scratches are observed along the sliding direction. The grinding induced grooves remain clearly visible and largely uninterrupted, while quite a significant amount of indentations is present on the worn surface.

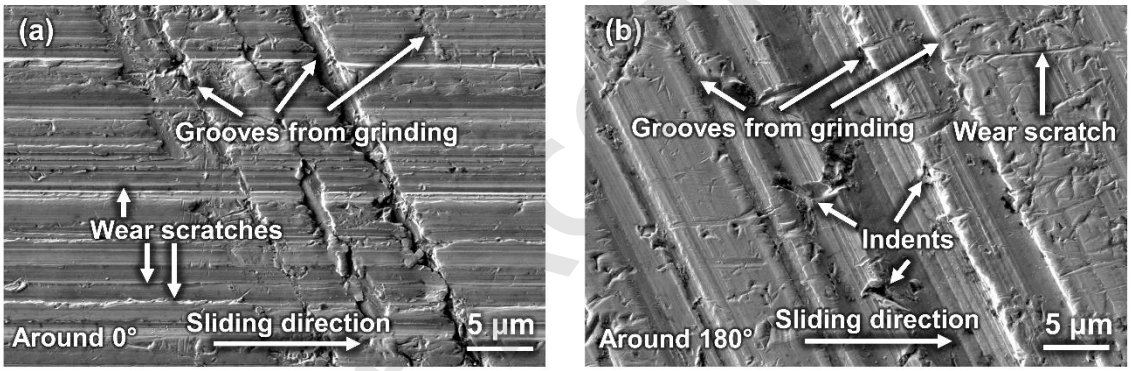

Fig. 7 SEM images of disk after tribological tests. (a) corresponds to the high friction region around 0°, as identified in the spatial friction map shown in Figure 4. In the direction parallel to sliding, dense and continuous wear scratches are clearly visible. (b) corresponds to the low friction region around 180°, where no continuous wear scratches are observed along the sliding direction.

3.5 Time frequency analysis

Fig. 8a presents the evolution of the friction force between 1700 s and 2300 s, along with the corresponding scalogram in Fig. 8b, capturing the transition from lubricated to abrasive wear conditions in both the time and frequency domains. After the introduction of the abrasive slurry at approximately 2000 s, the friction force did not increase immediately. Instead, a noticeable rise began at around 2080 s, where the friction force increased from approximately 0.07 N to 0.22 N by time stamp 2095 s. The sharp increase in friction force was accompanied by the emergence of pronounced

spectral features, most notably within the low-frequency range around 0.94 Hz and its harmonics (1.88 Hz and 2.82 Hz). In addition, intermittent high frequency components, particularly at approximately 47 Hz, a strongly amplified frequency component appears. In contrast, before the sharp rise in friction force, the wavelet spectrum showed only weak vertical streaks.

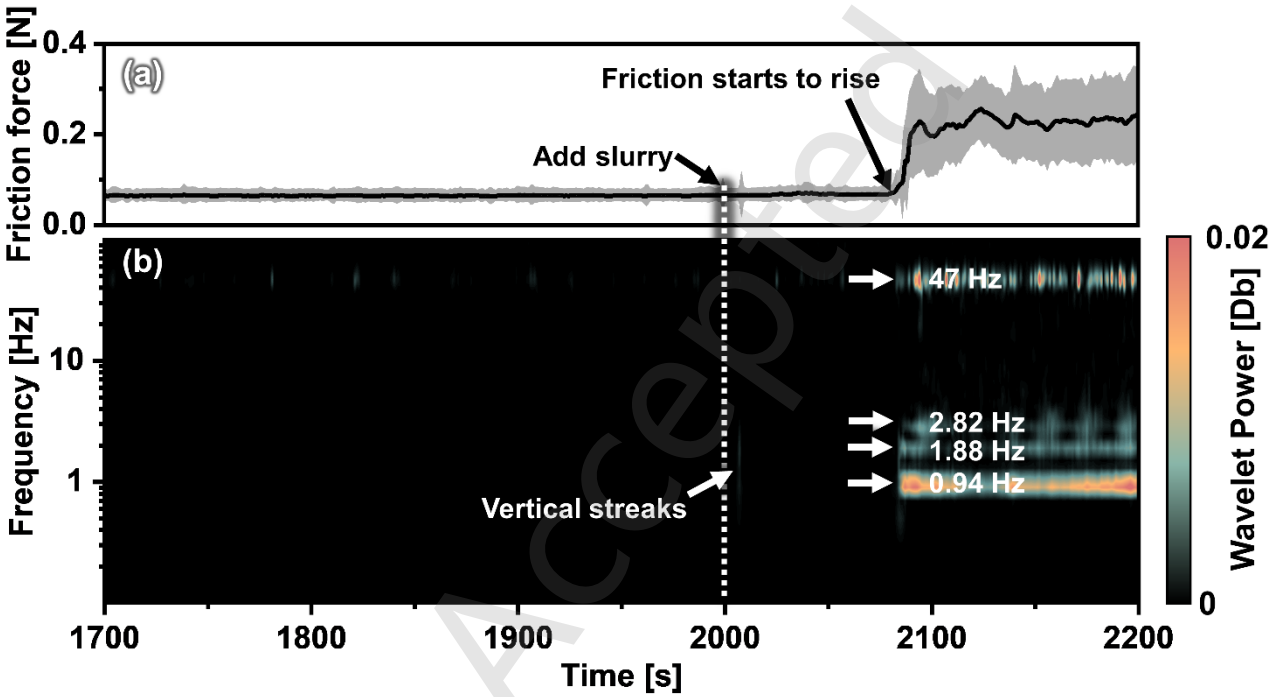

Fig. 8 Scalogram of the friction signal using continuous wavelet transform. (a) Evolution of the friction force between 1700 s and 2300 s, and (b) the corresponding scalogram of the signal shown in (a). Both plots share the same time axis. At 2000 s, an abrasive slurry was introduced to the system to induce abrasive wear. After the friction increase, distinct frequency features appear.

To better highlight the spectral distribution of frictional signals (in Fig. 9a) before and after the introduction of abrasive particles, the scalogram in Fig. 8b was normalized for each time slice individually, resulting in the normalized spectrum shown in Fig. 9b. This approach allows for clearer visualization of the relative power across different frequencies at each time point, independent of absolute power magnitudes.

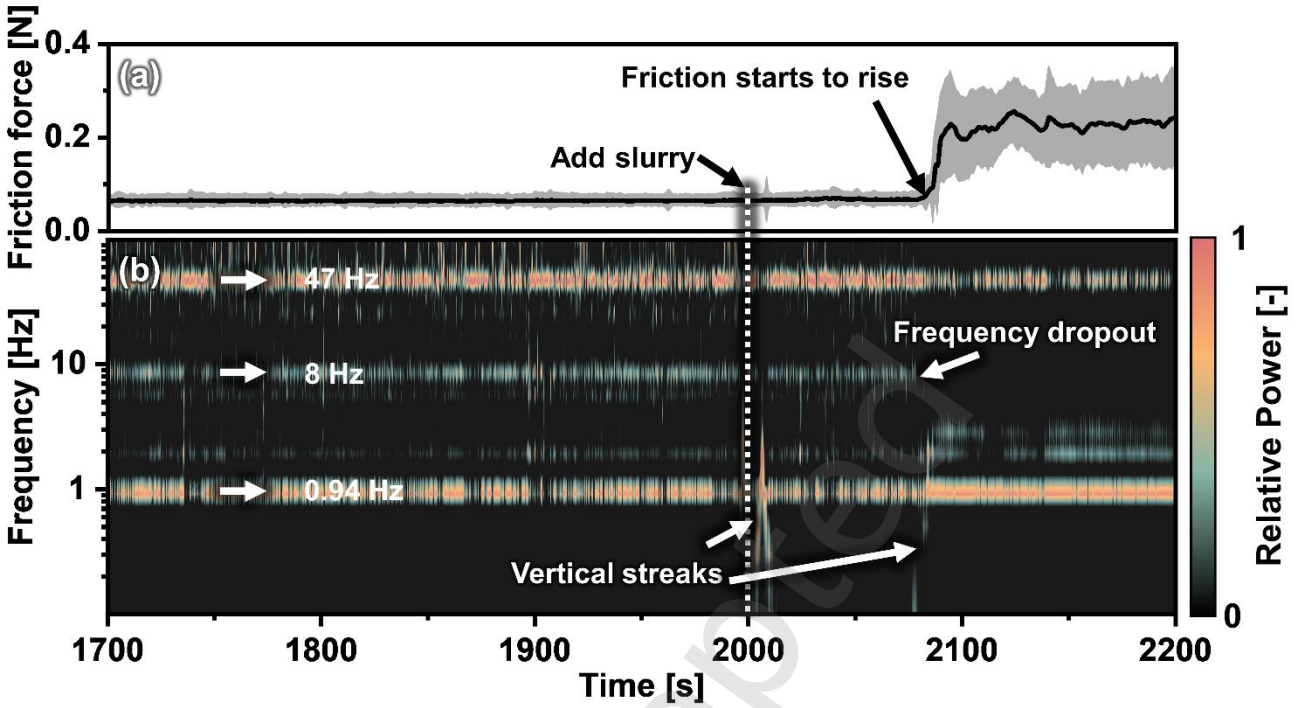

Fig. 9 Column wise normalized scalogram. (a) Evolution of the friction force between 1700 s and 2300 s. (b) Column wise normalized wavelet power spectrum (scalogram) of the friction signal shown in Fig. 8b. The normalized scalogram clearly reveals the frequency features both before and after the friction rise.

As shown in Fig. 9b, before the introduction of the abrasive slurry (at 2000 s), distinct frequency components were observed at 0.94 Hz and 47 Hz. At the onset of the friction increase, the intensity of the 0.94 Hz component became more pronounced, while the 47 Hz component weakened. Notably, immediately after the slurry was introduced, but before any significant change in friction, a series of strong vertical streaks appeared in the wavelet spectrum (at 2007 s), indicating broadband transient excitation. Similar vertical features were also observed shortly before the friction began to rise (at 2080 s). Additionally, the 8 Hz frequency component, present earlier in the test, ceased to be observable just before the onset of the friction increase (at 2080 s).

To ensure that the observed spectral signatures were physical phenomena rather than parameter dependent artifacts, sensitivity analysis was performed using the Morlet wavelet with a lower resolution (12 voices per octave) and the Morse wavelet with a higher resolution of 48 voices per octave, the results is presented in Supplementary Note 3.

4 Discussion

This study demonstrates how a friction system evolves from lubricated conditions to abrasive wear under continuous operation and reveals the correlations between these states. By analyzing friction, topography, and time frequency features, our work demonstrates that the onset of abrasive wear is preceded by measurable indicators in spatial, frequency, and time domains and can therefore be predicted.

4.1 Predicting friction and wear from the spatial domain

Conventionally, friction values under lubricated and abrasive wear conditions are rarely discussed together, as these regimes exhibit fundamentally different characteristics [25]. As shown in Fig. 3, the time-series data reveal that under lubricated conditions the friction force remains low and stable, with an average value of approximately 0.07 N and maximum fluctuations of about 0.03 N. In contrast, after the onset of abrasive wear, the friction force rises sharply and exhibits large amplitude fluctuations, reaching a value of around 0.25 N with maximum frictional fluctuations approaching 0.2 N. Under abrasive wear conditions, the observed frictional fluctuations originate from the nonuniform spatial distribution of friction across the disk, as also reported in a previous study [26]. However, what is particularly interesting is that even under lubricated conditions, where the overall friction level and its fluctuations remain low, spatial variations in friction are still evident. When the frictional data are examined with enough spatial resolution, both conditions exhibit remarkably similar distribution patterns. It is surprising that, despite the friction magnitudes differing by nearly an order of magnitude, the spatial trends remain comparable; for example, regions of high friction consistently appear around 0°. To ensure that the observed correlation is robust and not coincidental, a repeated experiment was performed in Supplementary Note 2, which consistently confirmed the similarity of the spatial trends across different tribological states.

In practical operation, regions of high friction are more likely to correspond to greater wear [27], which is consistent with the present observations. In Fig. 6b and c, the high friction area around 0° exhibits numerous wear scratches aligned parallel to the sliding direction, whereas in Fig. 6e and f such scratches are comparatively sparse. The higher resolution SEM images in Fig. 7 further confirm this difference. This, in turn, implies that the locations of more severe wear can be anticipated based on the friction distribution observed under lubricated conditions. The strong spatial correlation between the two regimes offers a potential approach to prevent localized tribological failures through predictive maintenance.

4.2 Failure diagnostics from the frequency domain

The application of continuous wavelet transform (CWT) analysis to the friction signal provided additional insight into the temporal evolution of friction and wear. In the present work, a continuous wavelet transform (CWT) with the Morlet mother wavelet was employed, as it offers an optimal compromise between time and frequency resolution, allowing accurate identification of transient features in nonstationary frictional signals [21, 28]. Following slurry introduction (at 2000 s, in Fig. 8a) to generate abrasive wear conditions, a latency of 80 s preceded the rapid friction increase (at 2080 s). From the onset of this friction increase (2080 s), pronounced spectral features can be observed in the scalogram (Fig. 8b), whereas before 2080 s, only faint vertical streaks are visible. This difference arises because both the friction force and its fluctuations under lubricated and abrasive wear conditions differ by nearly an order of magnitude, resulting in substantial disparities in wavelet power that make a direct comparison on the same scale challenging.

To address the above issue, a normalized scalogram was introduced. The normalized scalogram reveals pronounced changes in the frequency characteristics of the friction signal after the slurry was added, but before the friction force began to increase. This frequency response reflects the process of particle

transport and the gradual degradation of the lubricating film. Following injection, abrasive particles must first be transported from the injection point and entrained into the contact interface. As shown in Fig. 9b, even though the friction force did not change significantly immediately after the slurry introduction, a broadband transient excitation appeared at approximately 2007 s, indicating that individual particles had already begun to enter the contact and induce localized frictional perturbations. At this stage, the lubricated condition had not yet fully deteriorated, and these localized fluctuations were insufficient to immediately alter the macroscopic, time averaged friction force. Subsequently, particles accumulate at the interface, and as the concentration of 5 μm particles increases, the lubricated condition ultimately breaks down. At approximately 2080 s in Fig. 9b, the system transitions from a stable lubricated state to abrasive wear regime, resulting in a rapid rise in friction and the certain frequency dropout (e.g., the 8 Hz band in Fig. 9b). Integrating such a normalized scalogram into real-time monitoring systems could substantially enhance predictive maintenance capabilities, particularly when combined with machine learning algorithms capable of learning the statistical characteristics of pre-failure signals [29].

The features observed in the frequency domain also manifest correspondingly in the spatial domain. As shown in Fig. 3, the friction signal in the time domain remains stable under lubricated conditions. Before 2000 s, both the friction level and its fluctuations are low, and the frequency domain exhibits stable spectral features, as seen in Fig. 9. Consistently, the spatial distribution of friction is also stable; in Fig. 10a, the spatial friction patterns during 700-1000 s and 1800-1810 s show remarkable similarity. After the introduction of the abrasive slurry, the time domain friction (Fig. 3) around 2000 s exhibits no significant change, yet pronounced spectral features emerge in the frequency domain. Meanwhile, as shown in Fig. 10b, the addition of the abrasive slurry induces intense local variations in friction (e.g. around 90°) within a short period (2000-2010 s). These localized fluctuations likely disrupt the

previously stable spectral components, leading to the appearance of continuous vertical streaks in the frequency domain (in Fig. 9).

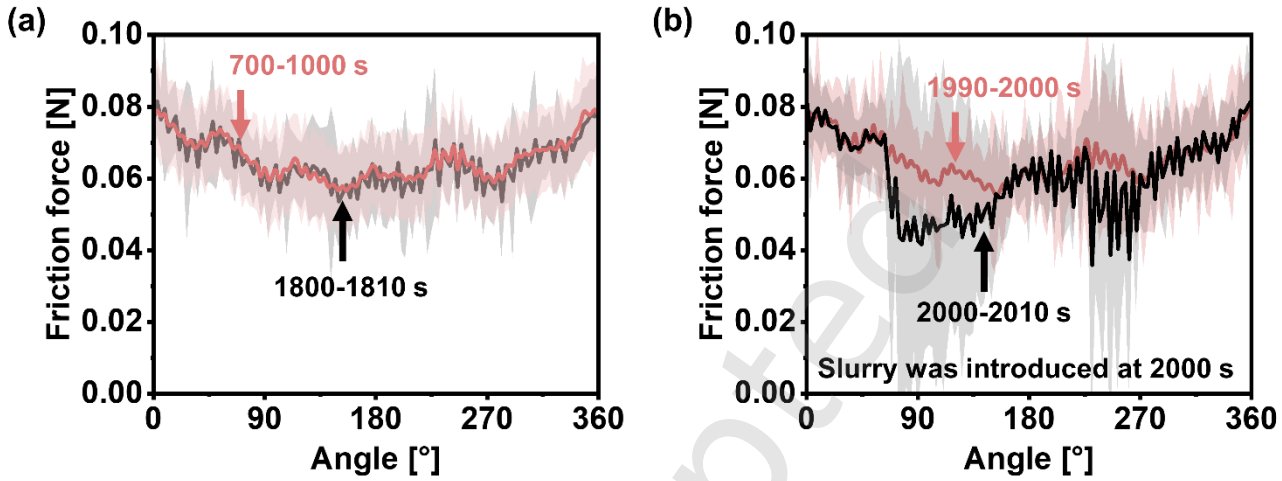

Fig. 10 Spatial domain friction force. (a) Under lubricated conditions, the spatial distribution of friction remains highly stable. The friction patterns between 700-1000 s and 1800-1810 s show remarkable similarity. (b) At 2000 s, the abrasive slurry was introduced, the addition of the abrasive slurry induces intense local variations in friction within a short period (2000-2010 s).

4.3 Predicting high friction before the onset of tribological contact

Along the sliding track of a uniformly prepared disk, the locations of the highest friction do not necessarily depend on roughness parameters like R_a and R_q [30, 31]. This observation is consistent with our findings in Fig. 5a, where the spatial distribution of friction appears to have no direct correlation with the surface roughness R_q. While this does not imply that traditional surface roughness evaluation is inadequate, but rather suggests that the effect of scale should not be overlooked when interpreting roughness [32, 33]. When examining the surface profile (a larger scale surface roughness) and friction along the entire sliding track, as shown in Fig. 5b, the highest friction coincides with a 2 μm surface protrusion around 0°.

However, a new issue emerges: another protrusion on the disk surface profile, located around 160°, does not correspond to a region of high friction. This discrepancy arises because whether a protrusion

results in high friction is often influenced by tilting introduced oscillations (in Fig. 2) during disk mounting [34]. While both the surface profile and the tilting induced oscillation caused by inclination are unique and consistently present, a recent finding [34] shows that it is possible to predict the locations of high friction based on their combined characteristics. One approach divides the sliding track into 120 sections and selects those simultaneously satisfying three physical conditions: a negative oscillation slope, an above average surface profile height, and a positive surface curvature. The resulting predictions are shown in Fig. 11.

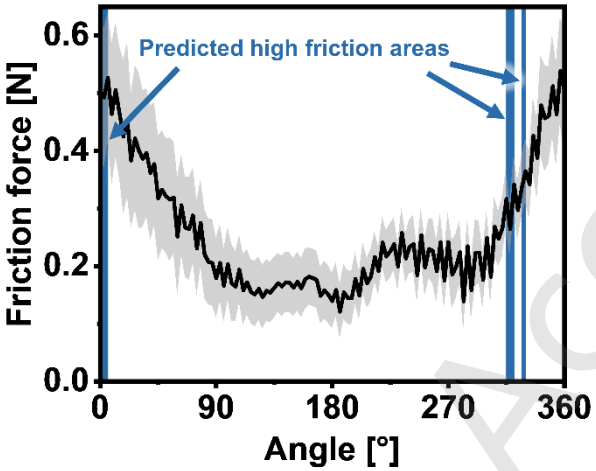

Fig. 11 High friction prediction. The black curve represents the spatial-domain friction under abrasive wear conditions, obtained from the time intervals of 2200-2500 s. The blue bands indicate the regions predicted to exhibit high friction. These predictions were generated using the previously published method [31], which divides the sliding track into 120 sections and selects those that simultaneously satisfy three physical conditions: a negative oscillation slope, an above average surface profile height, and a positive surface curvature.

In Fig. 11, the blue bands mark the regions predicted to exhibit high friction, and these predictions align closely with the locations where high friction and wear were experimentally observed (in Fig. 4 and Fig. 5). Notably, the prediction was made using only the data obtained before the tribological contact. This not only demonstrates the feasibility of the proposed approach but also underscores the inherent complexity of tribological systems. By integrating multidimensional information, such analyses bring us a significant step closer to successfully predicting friction.

5 Conclusions

This study employs a slightly modified commercial pin-on-disk instrument, with both contacting surfaces made of 100Cr6 bearing steel, to conduct a multidimensional investigation of the transition from a lubricated regime to abrasive wear under continuous operation. The results demonstrate that the onset of abrasive wear is preceded by clearly identifiable indicators.

Spatial domain analyses revealed that, despite the order of magnitude difference in friction between lubricated and abrasive wear conditions, the spatial distribution of friction on the disk remains remarkably consistent, enabling the use of lubricated-state data to anticipate and localize subsequent wear. Time frequency analysis further revealed that the initiation of abrasive wear is preceded by distinct transient spectral signatures, providing powerful early indicators for real-time diagnostics and predictive maintenance. Moreover, high friction regions can be predicted even before the tribological contact begins by combining the disk surface profile with disk tilting induced oscillations.

Overall, these findings demonstrate that tribological systems, while inherently multidimensional and highly complex, exhibit identifiable indicators across time, spatial, and frequency domains. Integrating these complementary dimensions, together with rapid advances in artificial intelligence, the development of fully predictive friction and wear models is becoming increasingly attainable.

6 Acknowledgements

The authors would like to thank N. Garabedian for lab help and discussions. CG acknowledges the financial support provided by European Research Council (ERC) grant (771237) and German Research Foundation grant (GR 4174/12) as well as funding through a Future Fields grant from KIT.

7 References

1. Holmberg K, Erdemir A (2017) Influence of tribology on global energy consumption, costs and emissions. Friction 5:263–284. https://doi.org/10.1007/s40544-017-0183-5
2. Bhushan B (2013) Introduction to tribology, Second edition. Wiley, Chicheste, West Sussex, United Kingdom
3. Rabinowicz E (1995) Friction and wear of materials, 2. ed. Wiley, New York, NY
4. Hutchings IM, Shipway P (2017) Tribology: friction and wear of engineering materials, Second edition. Butterworth-Heinemann, Oxford, England
5. Valizade N, Farhat Z (2024) A Review on Abrasive Wear of Aluminum Composites: Mechanisms and Influencing Factors. J Compos Sci 8:149. https://doi.org/10.3390/jcs8040149
6. Archard JF (1953) Contact and Rubbing of Flat Surfaces. Journal of Applied Physics 24:981–988. https://doi.org/10.1063/1.1721448
7. Shao Q (2005) Continuum model of abrasive layer in an abrasive wear test. Wear 259:36–43. https://doi.org/10.1016/j.wear.2005.03.015
8. Stachowiak GP, Podsiadlo P, Stachowiak GW (2006) Shape and texture features in the automated classification of adhesive and abrasive wear particles. Tribol Lett 24:15–26. https://doi.org/10.1007/s11249-006-9117-5
9. Gachot C, Rosenkranz A, Hsu SM, Costa HL (2017) A critical assessment of surface texturing for friction and wear improvement. Wear 372–373:21–41. https://doi.org/10.1016/j.wear.2016.11.020
10. Bedolla PO, Vorlaufer G, Rechberger C, et al (2018) Combined experimental and numerical simulation of abrasive wear and its application to a tillage machine component. Tribology International 127:122–128. https://doi.org/10.1016/j.triboint.2018.03.019
11. Paturi UMR, Palakurthy ST, Reddy NS (2023) The Role of Machine Learning in Tribology: A Systematic Review. Arch Computat Methods Eng 30:1345–1397. https://doi.org/10.1007/s11831-022-09841-5
12. Rosenkranz A, Marian M, Profito FJ, et al (2020) The Use of Artificial Intelligence in Tribology—A Perspective. Lubricants 9:2. https://doi.org/10.3390/lubricants9010002
13. Marian M, Tremmel S (2021) Current Trends and Applications of Machine Learning in Tribology—A Review. Lubricants 9:86. https://doi.org/10.3390/lubricants9090086
14. Garabedian NT, Schreiber PJ, Brandt N, et al (2022) Generating FAIR research data in experimental tribology. Scientific Data 9:315. https://doi.org/10.1038/s41597-022-01429-9
15. Holey H, Gumbsch P, Pastewka L (2025) Active learning for nonparametric multiscale modeling of boundary lubrication. Sci Adv 11:eadx4546. https://doi.org/10.1126/sciadv.adx4546
16. Marian M, Mursak J, Bartz M, et al (2023) Predicting EHL film thickness parameters by machine learning approaches. Friction 11:992–1013. https://doi.org/10.1007/s40544-022-0641-6
17. Kovalev A, Tian Y, Meng Y (2024) Prediction of ball-on-plate friction and wear by ANN with data-driven optimization. Friction 12:1235–1249. https://doi.org/10.1007/s40544-023-0803-1
18. Prost J, Boidi G, Lebersorger T, et al (2022) Comprehensive review of tribometer dynamics-Cycle-based data analysis and visualization. Friction 10:772–786. https://doi.org/10.1007/s40544-021-0534-0
19. Wu Z, Yin N, Wang W, et al (2026) Tribo-informatics approach for monitoring the coefficient of friction and its fluctuation in sliding contact based on sound and vibration multi-signals. Tribology International 214:111130. https://doi.org/10.1016/j.triboint.2025.111130

20. Baccar D, Söffker D (2015) Wear detection by means of wavelet-based acoustic emission analysis. Mechanical Systems and Signal Processing 60–61:198–207. https://doi.org/10.1016/j.ymssp.2015.02.012
21. Matsuo T (2005) Application of wavelet transform to control system diagnosis. In: IEE Seminar on Control Loop Assessment and Diagnosis. IEE, London, UK, pp 81–88
22. Sherrington I, Glavatskih S (2025) Tribotronic components: A revolution transforming machine elements into cyber-physical systems. Friction 13:9440987. https://doi.org/10.26599/FRICT.2025.9440987
23. Lilly JM, Olhede SC (2012) Generalized Morse Wavelets as a Superfamily of Analytic Wavelets. IEEE Trans Signal Process 60:6036–6041. https://doi.org/10.1109/TSP.2012.2210890
24. Torrence C, Compo GP (1998) A Practical Guide to Wavelet Analysis. Bull Amer Meteor Soc 79:61–78. https://doi.org/10.1175/1520-0477(1998)079<0061:APGTWA>2.0.CO;2
25. Mizuta K, Nishizawa Y, Sugimoto K, et al (2014) Evaluation of Friction Phenomena of Brake Pads by Acoustic Emission Method. SAE Int J Commer Veh 07:703–709. https://doi.org/10.4271/2014-01-2484
26. Li Y, Garabedian N, Schneider J, Greiner C (2023) Waviness Affects Friction and Abrasive Wear. Tribol Lett 71:64. https://doi.org/10.1007/s11249-023-01736-1
27. Lontin K, Khan M (2021) Interdependence of friction, wear, and noise: A review. Friction 9:1319–1345. https://doi.org/10.1007/s40544-021-0500-x
28. Liang J-W, Feeny BF (2005) Wavelet Analysis of Stick-Slip Signals in Oscillators With Dry-Friction Contact. Journal of Vibration and Acoustics 127:139–143. https://doi.org/10.1115/1.1891819
29. Zhao Y, Lin L, Schlarb AK (2023) Artificial neural network accomplished prediction on tribology – A promising procedure to facilitate the tribological characterization of polymer composites. Wear 532–533:205106. https://doi.org/10.1016/j.wear.2023.205106
30. Park S, Costa KD, Ateshian GA (2004) Microscale frictional response of bovine articular cartilage from atomic force microscopy. Journal of Biomechanics 37:1679–1687. https://doi.org/10.1016/j.jbiomech.2004.02.017
31. Qin W, Jin X, Kirk A, et al (2018) Effects of surface roughness on local friction and temperature distributions in a steel-on-steel fretting contact. Tribology International 120:350–357. https://doi.org/10.1016/j.triboint.2018.01.016
32. Pastewka L, Vakis AI, Aghababaei R, et al (2025) Modeling in tribology: Recent advances, applications, and open questions. Tribology International 111326. https://doi.org/10.1016/j.triboint.2025.111326
33. Pradhan A, Müser MH, Miller N, et al (2025) The Surface-Topography Challenge: A Multi-Laboratory Benchmark Study to Advance the Characterization of Topography. Tribol Lett 73:110. https://doi.org/10.1007/s11249-025-02014-y
34. Li Y, Gumbsch P, Greiner C (2025) Predicting Friction under Vastly Different Lubrication Scenarios

Yulong Li received his B.Sc. and M.Sc. degrees in Mechanical engineering at the Karlsruhe Institute of Technology (KIT), Germany. He is currently a postdoctoral researcher at KIT, where his research focuses on surface topography characterization and analysis. His research interests lie in applying data-driven approaches to uncover new insights into the role of surface topography in tribology.

Johannes Schneider. He received his diploma and Ph.D. degrees in mechanical engineering from the University of Karlsruhe, Germany, in 1992 and 1997 respectively. His current position is a Staff Scientist at the Institute for Applied Materials-Reliability and Microstructure (IAM-ZM) at the Karlsruhe Institute of Technology (KIT), Germany. His research interests include laser surface texturing and modification and its influence on friction and wear.

Christian Greiner. He obtained his master degree from the University of Stuttgart, Germany, in 2004 and his Ph.D. degree from the Max Planck Institute for Metals Research, Germany, in 2007. After a postdoc at the University of Pennsylvania, USA, he joined the Karlsruhe Institute of Technology (KIT), Germany, in 2010, where he became a full professor in 2021. He heads the Materials Tribology Group, mainly funded through a Consolidator Grant of the European Research Council (ERC). His research interests include microstructure property relations under a tribological load as well as bioinspired surface morphologies.